4-4-2023

Synthesis and Characterization of Humic/Melanin-like Compounds by Oxidative Polymerization of Simple Aromatic Precursors

Nastaran Khademimoshgenani
Michigan Technological University, nkhademi@mtu.edu

Sarah A. Green
Michigan Technological University, sgreen@mtu.edu

Recommended Citation

Article

Synthesis and Characterization of Humic/Melanin-like Compounds by Oxidative Polymerization of Simple Aromatic Precursors

Nastaran Khademimoshgenani * and Sarah A. Green *

Department of Chemistry, Michigan Technological University, 1400 Townsend Drive, Houghton, MI 49931, USA
* Correspondence: nkhademi@mtu.edu (N.K.); sgreen@mtu.edu (S.A.G.)

Abstract: Dissolved organic matter (DOM) is a complex mixture of naturally occurring organic molecules originating from multiple marine and terrestrial sources. DOM plays a significant role in water quality by affecting the photochemistry, trace metal transport, and acidity in aquatic systems. Understanding the chemical composition of DOM helps interpret the links between its optical properties and molecular structures. Currently, the molecular origins of the optical properties of DOM are not well-defined. In this study, we oxidize and initiate the polymerization of melanin precursors 1,8-dihydroxy naphthalene and 5,6-dihydroxy indole by the addition of hydrogen peroxide and/or with ultraviolet irradiation. Our goal is to evaluate the possibility of reproducing the optical signatures of DOM from simple aromatic precursors. Optical characterization shows an extreme shift of the absorbance to a featureless trend and broad fluorescence peaks (350–500 nm) like DOM. Electrospray ionization (ESI) and matrix-assisted laser desorption ionization (MALDI) mass spectrometry show evidence of oligomers with varying degrees of oxidation. The combination of our results shows that about 1–4 units of melanin oligomers with varying degrees of oxidation mimic the optical properties of DOM. Overall, our results strongly support the idea that simple precursors form oligomeric chromophores mimicking DOMs optical properties through simple oxidative steps.

Keywords: dissolved organic matter; fungal melanin; oxidation; oligomers

1. Introduction

The chemistry of soil organic matter (SOM) and the origins of its optical properties have been of great interest for decades [1,2]. SOM is the largest pool of organic carbon and a major contributor to carbon cycling [3–5]. As one of the main links between terrestrial and aquatic environments, the dissolved fractions of organic matter (DOM) contributes to nutrient balance in soils [6], as well as mobilizing metal ions [7,8], and controls the optical field in aquatic ecosystems [9]. One contributor to SOM, and potentially DOM, is fungal melanin, which produces dark-colored pigments in soil [10] with analogous optical properties to humic materials. As the largest pool of organic carbon in terrestrial environments, SOM consists of many different compounds sourced from plants and microbial organisms [11]. A part of SOM is or becomes soluble as dissolved organic matter (DOM), which is likewise a heterogeneous complex mixture with a range of molecular weights and functional groups. DOM is one of the largest dynamic pools of organic compounds in aquatic ecosystems [12]. Chromophoric dissolved organic matter (CDOM) is defined as the colored fraction of DOM that causes the brown color in streams and plays a significant role in optical dynamics and nutrient cycling of aquatic environments; therefore, understanding the characteristics of CDOM is crucial to water quality assessments and monitoring aquatic ecosystems [13–15]. Links between soil humic material and fungal melanin were suggested in the 1980s by Bell and Wheeler [16], and, indeed, the idea was raised as early as 1940 [17]. Fungal melanin is a heterogeneous group of dark-colored oligomers, which may contribute to dark-colored humic fractions of soil [11,16,18]. Although the distribution of fungal melanin in soil and

its impacts on carbon cycling of terrestrial environments have been studied recently [10,19], the potential of fungal melanin to contribute to humic fractions of soil or to DOM, and especially their optical properties, are not well constrained.

Fungal melanin and humic fractions of DOM show similarities in their optical properties (absorbance and fluorescence spectra), dark brown/black color, and categories of building units (aromatic structures). Both fungal melanin and HA are presumably associated with various phenols, amino acids, proteins, carbohydrates, and lipids [16,20]. Because of their similarities and the contributions of fungal melanin to humic substances, Bell and Wheeler suggested in 1986 that soluble fractions of fungal melanin could contribute to the dark brown color of the HA fraction of DOM [16]. Molecular formulas and mass ranges of the soluble fractions of typical melanin structures and humic substances show some similarities [21,22]. The main building block of eumelanin is dihydroxy indole (5,6-DHI), and 1,8-dihydroxy naphthalene (1,8-DHN) is the precursor for fungal melanin (allomelanin) (Scheme 1) [20]. Isolation, purification, and structural characterization of melanin polymers have encountered challenges such as insolubility, resistance to chemical treatments, and "molecular disorder" of the oligomeric units of melanin [20,23]. Similarly, defining the molecular properties of HA has been challenging due to their innate heterogeneity as well as their dynamic nature as they undergo photochemical and microbial degradations [24,25].
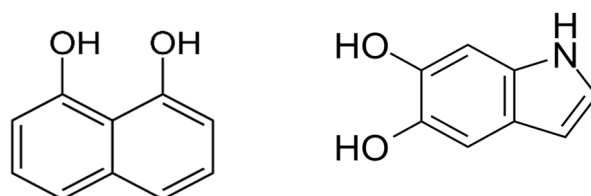
Scheme 1. The chemical structures of the two precursors employed in this study, 1,8-dihydroxy naphthalene (DHN) (**left**) and 5,6-dihydroxy indole (DHI) (**right**).

UV-visible spectroscopy is a versatile analytical technique that has been used to characterize both DOM and melanin. Absorption of DOM and its humic fractions is attributed to charge transfer (CT) resulting from electronic interactions between electron-donating and accepting groups [26]. Compared to well-defined absorption patterns of individual molecules, electron donor-acceptor CT complexes in humic substances result in a featureless spectrum with a broad appearance [27]. Similarly, the broad absorption spectrum of melanin is attributed to aggregation and intramolecular stacking of chromophores [28]. Computational studies have reproduced observed DOM absorption spectra from calculated spectra of model compounds to demonstrate that the superposition of chromophores, with or without CT interactions, can reproduce observed absorption spectra [29]. Compounds such as coumarin, flavone, and other quinone and phenol-based structures were used to model the absorption spectrum of DOM, with the assumption that DOMs absorption spectrum represents the sum of the absorption spectra of its components [29]. Modeling the intermolecular CT interactions within DOM molecules shows similarities in structural properties to melanin pigments [29]. As a computational modeling approach to understand the behavior and optical properties of eumelanin, Wang generated a virtual library of several hundred dimers of DHI and its oxidation products. This study found that some oxidized DHI dimers can give absorption bands >600 nm [30].

As a complementary approach to UV-visible spectroscopy, fluorescence spectroscopy monitors the emission of photons when electronically excited species return to their ground state. For CDOM, the excited charge-transfer complexes show a broad emission spectrum, which shifts to the red with increasing excitation wavelengths, and an average quantum yield of approximately 1% [27]. Melanin shows similar fluorescent characteristics, though with a smaller quantum yield of ≈0.1%, and because of its extremely low quantum yield, melanin has often been described as non-fluorescent [31–33]. These features of melanin have been attributed to a "stacked oligomer" structure [34], which means that the oligomeric

units of melanin with different sizes act as emitting species interacting with each other upon excitation and generating fluorescence signals [31,34]. The optical trends of melanin, such as broad ("enveloping") fluorescence, are also explainable by the "superposition model" proposed for CDOM, suggesting that the sum of multiple chromophoric moieties results in broad emission maxima [35].

Reduction treatments have been used to reveal the significant role of quinone and aldehyde/ketone fractions of CDOM, explained by the CT model [35,36]. Borohydride is known to reduce both aldehyde/ketones and quinone fractions, whereas dithionite selectively reduces quinones [37]. Borohydride reductions help gain insights into the carbonyl-containing portions of CDOM, while dithionite treatments reveal information about the quinone/hydroquinone contents of CDOM specifically [36,37]. The common responses to reduction include a significant loss of absorbance and a fluorescence gain with a blue shift. Del Vecchio et al. found that using dithionite for selective reduction of quinones resulted in a negligible change of absorbance and little to no changes in fluorescence for the SRFA standard; however, for the standard Elliot soil humic acid (ESHA), a significant fluorescence gain in the visible region with a blue shift was shown [36]. The ESHA response could be suitable for comparison to our model fungal melanin products [10]. In the present work, the applicability of the CT model was investigated by using borohydride and dithionite treatments and investigating the responses of our aged 1,8-DHN and 5,6-DHI samples. Perhaps, based on the contribution of fungal melanin to SOM [10], it could be expected that our aged products of oxidized 1,8-DHN and 5,6-DHI show similar changes to the ESHA standard.

To elucidate the origins of the optical properties of CDOM, experimental modeling approaches have used aromatic structures to mimic the optical properties of humic fractions of CDOM. McKay demonstrated that autoxidized hydroquinone compounds reproduce similar absorbance and fluorescence spectral trends of CDOM [35]. McKay also investigated the effects of borohydride treatments and compared the absorbance and fluorescence patterns to standard CDOM isolates such as SRFA, which revealed similar patterns of absorption loss and blue-shifted enhanced fluorescence. This supported the CT model and the significant role of aromatic compounds contributing to the optical characteristics of CDOM, although no molecular characterization (e.g., mass spectrometry) was carried out to investigate the molecular trends of oxidized humic-like products from hydroquinone and CDOM [35]. Yakimov et al. showed that a heterogeneous mixture of aromatic compounds such as dihydroxy benzoic acid (DHB) and tryptophan (Trp) reproduces humic optical properties through oxidation [38]. In this study, photo-oxidation and ozonation of Trp and DHB generated oxidized products with similar UV-visible absorbance, spectral slope, and fluorescence trends compared to SRHA. Reduction treatments resulted in an overall loss of absorption and fluorescence gain, indicating the consistency of humic-like optical properties with the CT model; however, some discrepancies were observed in absorption trends of reduced DHB, showing distinct absorption maxima instead of a humic absorption trend [38]. In the present study, fungal melanin precursors are used to model humic optical properties of CDOM through oxidative polymerization and study the optical and molecular trends of the model fungal melanin compounds. The present study will address the following: (1) Providing further evidence that humic optical trends of CDOM can be mimicked by simple aromatic structures and developing comparable molecular trends to HA. (2) Linking fungal melanin compounds to humic fractions of CDOM, considering the contributions of melanized fungal communities in soil to organic matter and potentially its colored soluble fractions (CDOM).

Mass spectrometry has proven to be a powerful analytical approach to identify molecular signatures and molecular formulas of natural organic matter [39–41]. Mass spectrometry of both DOM and melanin compounds has employed ionization techniques such as electrospray ionization (ESI) [42,43] and matrix-assisted laser desorption ionization (MALDI) [44,45]. Common mass spectra of DOM are composed of thousands (5000–10,000) of m/z peaks detected in a mass range of 100–1000 Da, with most peaks below 600 Da [39].

Likewise, ESI mass spectrometry shows masses for fungal DHN-melanin in the range of 300–500 Da [43], while for DHI-melanin, the scan range has been expanded from 100 to 2500 Da to include higher numbers of monomeric units [46]. For both DOM and melanin, complementary analytical techniques such as elemental analysis alongside ESI and MALDI-MS are needed for the prediction of molecular formulas and possible structures [39,43]. Mass spectrometry of melanin helps us understand chemical events during or after polymerization; however, it has been extremely challenging to assign any molecular formula to these compounds as a consistently defined formula. One of the complications is that the average mass of fungal melanin, depending on the fungal species and the number of oligomeric units (4–8 units), may vary [47,48]. Therefore, for both DOM and melanin, comparing ranges of the most common molecular formulas and their molar ratios is a useful approach [41,49,50]. Graphical tools such as van Krevelen diagrams and Kendrick mass defect (KMD) plots have been used to help visualize the molecular characteristics of complex melanin polymers and humic fractions of DOM [39,49,51].

Here we employ optical measurements and mass spectrometry to probe similarities and differences between DOM and lab-produced mixtures generated from the oxidation of melanin precursors (Scheme 1). In this study, we hypothesize that oxidative polymerization of simple melanin precursors such as 1,8-DHN and 5,6-DHI produces oxidized oligomers that can mimic the humic-like optical properties of the colored fraction of DOM (CDOM). In this work, we compare the optical and molecular properties of these model compounds to those of humic fractions of CDOM. For this strategy, we selected simple molecular precursors, typically used to synthesize model melanin compounds, to undergo photo-oxidation and oxidative polymerization to develop humic-like properties. UV-visible and fluorescence spectroscopy are used in combination with ESI and MALDI mass spectrometry to characterize the products of the oxidative polymerization and aging process for 1,8-DHN and 5,6-DHI precursors. In addition, the responses of the oxidized and aged products of 1,8-DHN and 5,6-DHI to reduction treatments are tested to investigate the applicability of the CT model to explain the reproduced humic optical trends.

2. Materials and Methods

All chemicals, including 1,8-dihydroxy naphthalene (1,8-DHN), 5,6-dihydroxyindole (5,6-DHI), sodium borohydride, sodium dithionite, acetonitrile, and hydrogen peroxide 30% (9.8 M) were purchased from Sigma Aldrich (St. Louis, MI, USA). Deionized water was from a Barnstead™ E-Pure™ Ultrapure Water Purification System. Stock solutions of both 1,8-DHN (DHN) and 5,6-DHI were prepared by dissolving the precursor in acetonitrile (ACN). 1,8-DHN samples were prepared by dissolving 0.056 g of solid 1,8-DHN in 15 mL ACN (0.023 M). 5,6-DHI samples for the UV irradiation experiments were prepared by dissolving 0.013 g of solid 5,6-DHI in 11 mL of ACN (0.008 M). The 10% ACN was a compromise to maintain the solubility of both 1,8-DHN and 5,6-DHI precursors while achieving 90% aqueous solutions. ACN is considered photochemically inert and relatively resistant to radical reactions; therefore, ACN was not expected to alter the composition of the samples. Stocks were diluted in water by a 1:10 ratio for irradiation in the UV reactor (Table 1). The concentrations of the samples prepared for UV irradiation are included in Table 1. For optical measurements of each sample, 50 μL of the original solution was diluted with water to 10 mL. The pH values of the prepared samples are 1,8-DHN: pH = 6.0 and 5,6-DHI: pH = 6.5.

Table 1. Composition of samples, concentration, duration of UV exposure, and storage in the dark.

Compound	Concentration in 1:10 ACN: Water Mixture	H_2O_2	UV Irradiation Time	Storage in the Dark
1,8-DHN	0.0023 M	___	3 h	10 days
5,6-DHI	0.0008 M	___	3 h	4 days
1,8-DHN	0.0023 M	5% *v/v*	3 h	10 days
5,6-DHI	0.0008 M	5% *v/v*	3 h	4 days

2.1. Photochemical Oxidation in Ultraviolet (UV) Reactor

Samples were irradiated in a Rayonet UV reactor model RMR-600 with an RMR 3500A lamp (350 nm) (Branford, CT, USA). 1,8-DHN and 5,6-DHI samples were prepared as above with or without the addition of 5% hydrogen peroxide; H_2O_2 was added to accelerate oxidation. Four replicate experiments were carried out to determine the amount of H_2O_2 to accelerate oxidation with little to no alterations to the optical trends while being able to investigate the effects of aging of the samples over time. All samples were exposed to UV irradiation for 3 h only to initiate the oxidative polymerization, with a measurable change of UV-visible absorption. Afterward, samples were stored in a dark cell at room temperature for 4–10 days, and absorbance and fluorescence spectra were collected at regular intervals. The optical measurement intervals for 1,8-DHN were continued to the point when an approximately featureless optical trend was achieved, and no significant changes were observed from day 10 up to ~6 months. The 10-day aged samples were used for optical and mass spectrometry characterization to avoid challenges of insoluble precipitates formed over longer periods. The optical measurements for aging 5,6-DHI ended earlier than expected (~4 days) due to the formation of insoluble precipitates.

Mass spectrometry analysis was done for untreated 1,8-DHN and 5,6-DHI and the aged UV-irradiated samples stored in the dark. Parameters for the UV irradiation experiments for 1,8-DHN and 5,6-DHI samples are shown in Table 1.

2.2. Ultraviolet (UV)-Visible Spectroscopy

Absorbance spectra were collected by Shimadzu UV-3600 plus UV-VIS-NIR spectrophotometer (Tokyo, Japan) in a Starna cell Spectrosil Far UV quartz with a useable range of 170 to 2700 nm. The wavelength range was 260–600 nm. The sampling interval was 0.5 nm with a slit width of 2 nm.

Specific UV absorbance (SUVA) estimates were made on the oxidized and aged 1,8-DHN (~6 months old). The absorbance values were normalized based on the estimated dissolved organic carbon (DOC) per mg/L, assuming no remineralization. This measurement was not carried out for aged 5,6-DHI samples due to the formation of dark insoluble precipitates rather quickly (~4 days of aging).

2.3. Fluorescence Spectroscopy

Excitation and emission spectra were measured by a Horiba fluoromax-4 spectrofluorometer (Piscataway, NJ, USA). For emission spectra, three spectra were collected for 1,8-DHN consecutively at excitation wavelengths of 302 nm, 318 nm, and 332 nm. Similarly, the emission spectra for 5,6-DHI samples were collected at the excitation wavelength of 298 nm. Excitation-emission matrix (EEM) spectra were collected over the excitation range of 300 to 450 nm to demonstrate emission spectra and fluorescence intensities over a broad range of excitation wavelengths. To increase the consistency of our comparison, the original three-dimensional contour plots of EEM were flattened into a two-dimensional plot. All measurements were recorded with a 1 nm slit and an integration time of 0.1 s.

2.4. Reduction Treatments

The aged 1,8-DHN and 5,6-DHI (~6 months old) were reduced by adding sodium borohydride and sodium dithionite. Prior to borohydride treatments, pH adjustments were considered by using NaOH to reach pH 7.0; however, pH levels of both aged 1,8-DHN and 5,6-DHI were 7.0. Absorbance and fluorescence were recorded prior to reduction. For reduction treatments, according to [52], 5 mg of sodium borohydride was added to 5 mL of each 1,8-DHN and 5,6-DHI sample. Similarly, 5 mg of sodium dithionite was added to 5 mL of each 1,8-DHN and 5,6-DHI sample. After 48 h, the absorbance and fluorescence of the samples were collected. The same procedure was repeated by three replicates. The absorbance and fluorescence spectra were collected according to Sections 2.2 and 2.3.

2.5. Mass Spectrometry

Mass spectra were collected with a Thermo Scientific Orbitrap Elite Mass Spectrometer (Waltham, MA, USA) with a resolution of 240,000 and a mass range of 100–800 Da. One hundred μL of analyte were injected for each analysis, and 150 scans were combined for each sample. ESI in negative mode was selected as the ionization technique. In addition, MALDI-MS analyses were conducted on Bruker Microflex LRF (Billerica, MA, USA) instrument. For MALDI-MS, the selected matrix was 2,5-dihydroxybenzoic acid (DHB), and the MALDI target was MSP 96 polished Steel.

Mass Spectrometry Analyses and Formula Assignments:

The software package MFassignR was employed for molecular formula assignment [53]. The molecular formulas are assigned to the ion m/z values by using the main elements C, H, and O, while the user is also able to include heteroatoms such as N. Common formula extensions, such as CO_2 and H_2O, are available to help reduce the number of ambiguous formulas, by including surrounding peaks and their mass differences with the selected ion, resulting in selecting only the most likely molecular formulas [53]. This software includes noise estimation, recalibration for mass measurements, and molecular formula assignment with necessary extensions. As a part of data analysis, the reconstructed mass spectra alongside Kendrick Mass Defect (KMD) plots and van Krevelen diagrams were plotted for each sample. KMD plots indicate a noise estimation with low-signal noise coming from the instrument and higher signals representing the analyte itself, and van Krevelen diagrams show the molar ratios of hydrogen-to-carbon (H/C) versus oxygen-to-carbon (O/C) for the most common molecular formulas [53].

3. Results

3.1. Optical Properties

3.1.1. Absorbance Spectra

Figure 1 shows the absorbance spectra for 1,8-DHN and 5,6-DHI samples with and without 5% H_2O_2. The spectra were collected before UV irradiation, after 3 h of irradiation, and after aging in the dark for 4 days or 10 days for 1,8-DHN and 5,6-DHI, respectively. 1,8-DHN initially shows three distinct absorption peaks at 302, 318, and 332 nm. Immediately after UV irradiation and for days 1–6 of the aging process, all absorption peaks were still present; however, they continuously decreased in intensity. Gradually, the distinct peaks disappeared and turned into a featureless and broad absorbance spectrum (after day 7). 5,6-DHI samples showed a primary absorbance peak at 298 nm, which decreases during the process of oxidation and aging. Eventually, its absorbance spectrum also becomes featureless. For 5,6-DHI samples, the absorbance measurements were stopped after 4 days because of the formation of insoluble dark-colored precipitates. A concomitant increase in absorbance was observed for all samples in the range of 350–500 nm. In both cases, oxidized materials show absorbance exponentially decreasing toward longer wavelengths, resembling the spectra of humic substances. Figure 1 insets show the spectral slopes for aged 1,8-DHN and 5,6-DHI, which can be compared to Suwannee River HA (SRHA) as the standard sample (Figure S3). Aged 1,8-DHN samples with no H_2O_2 showed a log-linear decrease of absorption with a similar absorption slope (−0.011) to aged 5,6-DHI samples with no H_2O_2 (−0.010), whereas the spectral slope of SRHA is slightly steeper (−0.017) (Figure S3). The spectral slope of aged 5,6-DHI with 5% H_2O_2 was −0.013, the closest value to standard SRHA among all four samples. Changes in absorbance at 350 nm and 400 nm plotted over time show an overall increase of absorbance at 350 and 400 nm for both samples (Figure S1). Comparing the samples with and without 5% H_2O_2 shows that adding H_2O_2 significantly increased the absorption gain at 350 and 400 nm over time for both 1,8-DHN and 5,6-DHI samples (Figure S1). Figure S2 shows the absorbance spectra over time, noting: (1) The optical measurement intervals ended after reaching a featureless spectrum (humic-like), while no significant changes in absorption trends were observed

after 10 days up to 6 months of aging. (2) The optical measurements for aging 5,6-DHI ended earlier than expected (~4 days) due to the formation of insoluble precipitates.
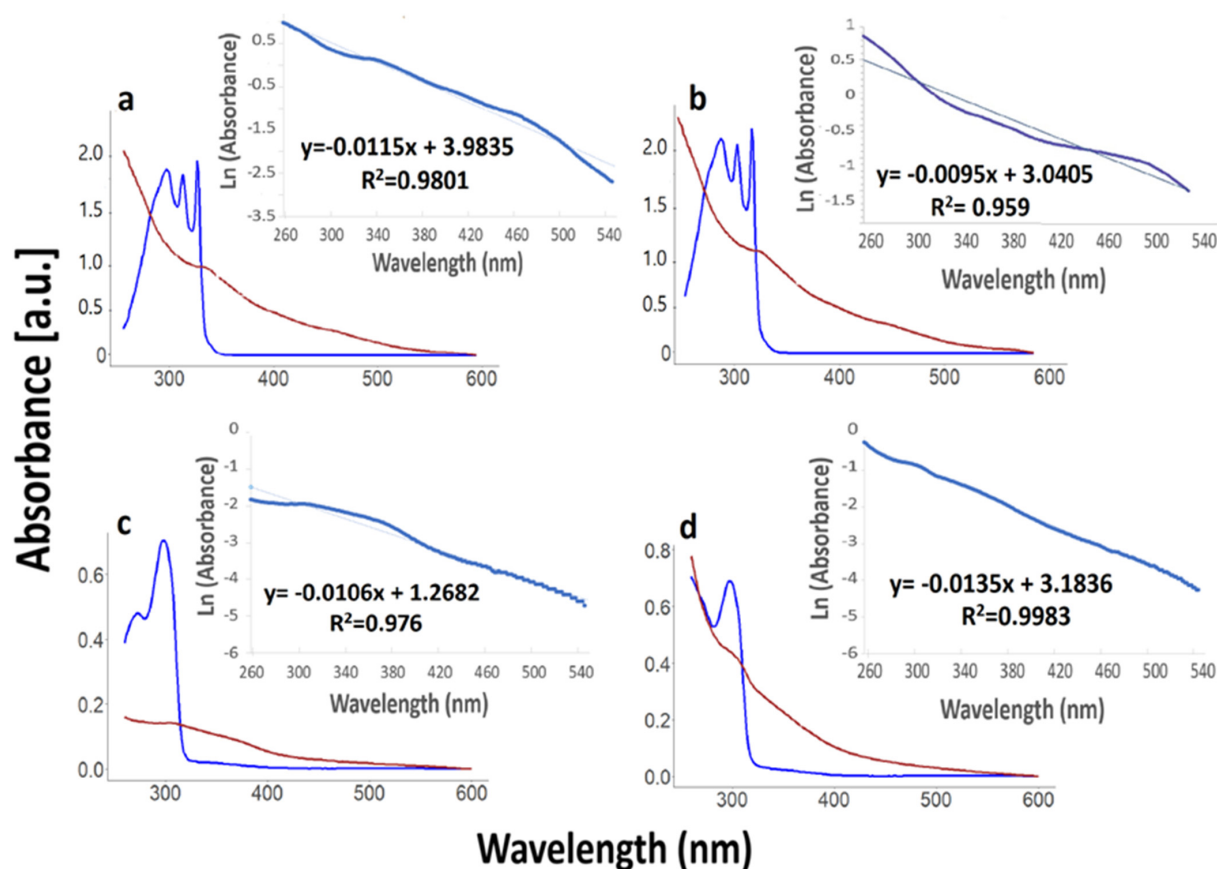
Figure 1. Absorbance spectra 1,8-DHN (**a**) and 1,8-DHN with 5% H_2O_2 (**b**), 5,6-DHI (**c**), and 5,6-DHI with 5% H_2O_2 (**d**). (Blue): initial 1,8-DHN or 5,6-DHI. (Brown line): After UV irradiation and 10 days aging for 1,8-DHN and 4 days aging for 5,6-DHI. All samples were diluted in water by 1:20. Insets: Log-linear plots of absorbance for oxidized/aged 1,8-DHN (**a**) with a spectral slope of −0.011, and 1,8-DHN with 5% H_2O_2 (**b**) with a spectral slope of −0.0095, 5,6-DHI (**c**) with a spectral slope of −0.010, and 5,6-DHI with 5% H_2O_2 (**d**) with a spectral slope of −0.013. The solid lines represent the log-linear absorption trends for each sample, and the dashed lines represent the best fitted line according to the calculated equations demonstrated on each linear plot. Original 1,8-DHN solution: pH = 6.0, original 5,6-DHI solution: pH = 6.5, aged 1,8-DHN: pH = 7.0, aged 5,6-DHI: pH = 7.0.

As a further comparison with humic substances, specific absorbance (absorbance per mg carbon) was estimated for the irradiated aged 1,8-DHN, as described in Section 2.2. Figure S4 shows the specific absorbance for aged 1,8-DHN samples in the wavelength range of 200 to 600 nm. The specific UV absorbance at 254 nm (SUVA) for 1,8-DHN samples was 7.70 L mg^{-1} m^{-1}. SUVA was not measured for aged 5,6-DHI samples due to the overall insolubility of the dark precipitates formed during the oxidation and aging process.

3.1.2. Fluorescence Spectra

Figure 2 shows the emission plots for 1,8-DHN and 5,6-DHI samples with/without 5% H_2O_2. Figure S5 shows the flattened emission spectra for the Suwannee River HA sample, compared to the emission spectra for 5,6-DHI and 1,8-DHN samples. For all samples, the fluorescence intensity decreases after UV irradiation, and it continues to decrease during 10 days of storage in the dark. The number of days for fluorescence measurements of 5,6-DHI samples was shortened due to the formation of insoluble black precipitates. Figure 2 shows that for samples without H_2O_2, the peak shapes remained the same (compared to

normalized lines), but their intensities decreased substantially. 1,8-DHN samples with 5% H_2O_2 showed new broad, red-shifted peaks (Figure 2). The emission spectrum for 5,6-DHI with a 5% H_2O_2 sample similarly shows a shift towards red wavelengths. These emission trends resemble the humic emission spectra (Figure S5).
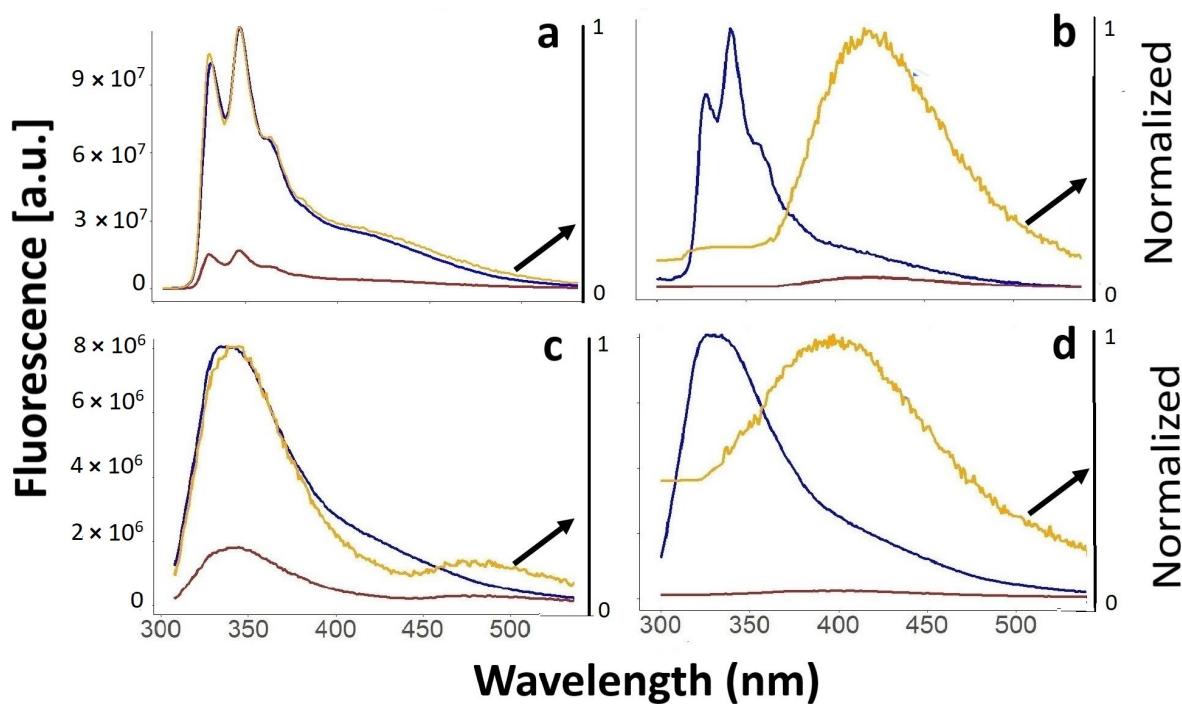
Figure 2. Emission spectra of 1,8-DHN (**a**) and 1,8-DHN with 5% H_2O_2 (**b**), 5,6-DHI (**c**), and 5,6-DHI with 5% H_2O_2 (**d**), (Blue): untreated; (Brown): after UV irradiation and 4 or 10 days of storage for 5,6-DHI and 1,8-DHN, respectively. (Light orange) normalized intensity for aged samples to compare peak shapes (normalized version of brown-colored spectra, marked by the black arrows). All samples were diluted in water by 1:20. For 1,8-DHN λ_{ex} = 302 nm, for 5,6-DHI λ_{ex} = 298 nm. Original 1,8-DHN solution: pH = 6.0, original 5,6-DHI solution: pH = 6.5, aged 1,8-DHN: pH = 7.0, aged 5,6-DHI: pH = 7.0.

Figure S5 shows emission spectra for a range of excitation wavelengths (300–550 nm) for 1,8-DHN and 5,6-DHI samples to demonstrate the red-shifted peaks like Figure 2 over a broad range of excitation wavelengths. The fluorescence emission spectra for aged 5,6-DHI shows two broad peaks at 420 nm and 525 nm that are shifting to longer wavelengths. For aged 1,8-DHN samples, the maximum peaks shift from 450 nm at the excitation wavelength of 300 nm to 525 nm. This plot shows a similar trend compared to the Suwannee River HA emission spectra in Figure S5.

3.2. Mass Spectrometry Results

3.2.1. ESI-MS Results

The negative-mode ESI mass spectrometry results for 1,8-DHN samples are shown in Figures 3 and 4. These mass spectrometry results show evidence of 1,8-DHN molecules being dominant in oxidized samples. Figure 3 shows the highest abundance peaks with m/z: 159.04 for negatively charged 1,8-DHN ions and m/z: 148.04 for negatively charged 5,6-DHI ions. The formation of ions with higher masses compared to the original precursors is demonstrated in all mass spectra; however, 1,8-DHN with 5% H_2O_2 shows four distinct clusters in its mass spectra as evidence of oligomerization (tetramers) (Figure 3e). Negative ESI results for 1,8-DHN samples with H_2O_2 show evidence of tetramers formed as new clusters in KMD plots (Figure S6). The van Krevelen diagrams (Figure 4) show that the original 1,8-DHN precursor has O/C = 0.2 and H/C = 0.8, and the 5,6-DHI precursor has

O/C = 0.25 and H/C = 0.875. Figure 4 shows several data points for both samples with higher O/C indicating evidence of oxidation. Oxidized samples have increased O/C (or decreased H/C) (Figure 4). Figure S6 shows the formation of higher ion masses compared to the original masses of the precursors, 160.17 g/mole for 1,8-DHN and 149.14 g/mole for 5,6-DHI in KMD plots. Figure 3 shows the mass spectra with higher m/z for the detected ions, compared to the original 5,6-DHI with m/z of 149.14. In addition, Figure 4 shows evidence of high degrees of oxidation since the original O/C ratio for 5,6-DHI is equal to 0.25, and we can see higher ratios of O/C values that are mostly detected within the range of 0.5 to 1.5. Tables S1 and S2 summarize the molecular formula assignments for the marked m/z peaks in the mass spectra of aged 1,8-DHN and 5,6-DHI.
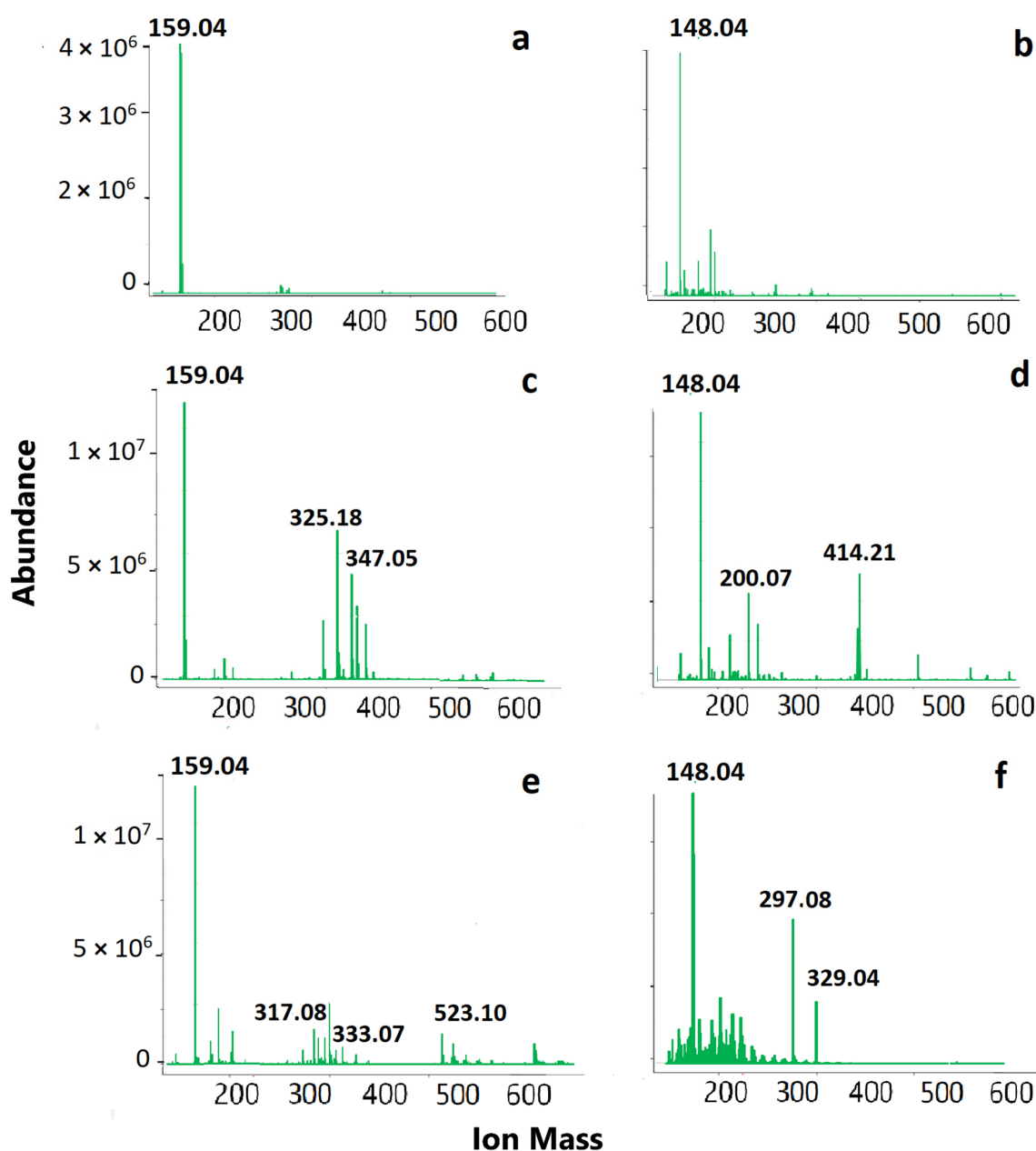
Figure 3. Mass spectra for original (non-irradiated) 1,8-DHN (**a**) and 5,6-DHI (**b**), post-irradiation samples: 1,8-DHN (**c**), and 5,6-DHI (**d**), 1,8-DHN with 5% H_2O_2 (**e**), 5,6-DHI with 5% H_2O_2 (**f**) in (-) ESI mode. All samples were diluted in water by 1:20. Original 1,8-DHN solution: pH = 6.0, original 5,6-DHI solution: pH = 6.5, aged 1,8-DHN: pH = 7.0, aged 5,6-DHI: pH = 7.0. m/z values are indicated in each mass spectrum.
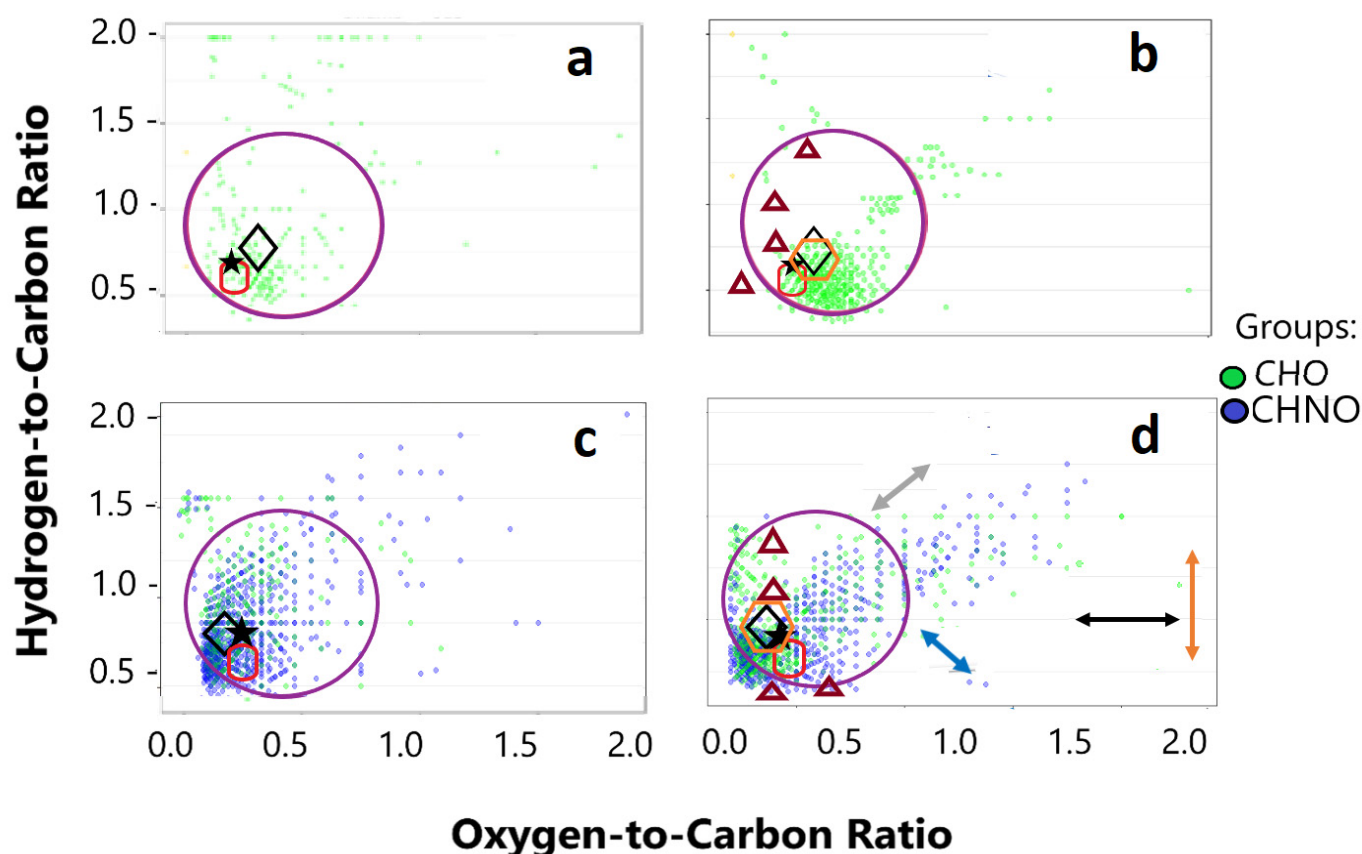
Figure 4. van Krevelen diagrams for 1,8-DHN (**a**) and 1,8-DHN with 5% H_2O_2 (**b**), 5,6-DHI (**c**), and 5,6-DHI with 5% H_2O_2 (**d**), in (-) ESI mode. All samples were diluted in water by 1:20. Red-colored regions show the average molar ratios for DHN/DHI-melanin. Purple circles show molar ratios for standard SRHA/SRFA. Black-colored diamond shapes show the original precursor's molar ratios for each precursor. The colored arrows represent suggested reaction pathways, black: oxidation/reduction, orange: hydrogenation/dehydrogenation, blue: methylation/demethylation (possibly polymerization), and grey: hydration/condensation [51]. The black star in each diagram marks the molar ratios for dimers, H/C: 0.635, O/C: 25 for 5,6-DHI dimer, H/C: 0.6, O/C: 0.2 for 1,8-DHN dimer. The orange hexagon shows the molar ratio ranges for the most abundant assigned formulas in Tables S1 and S2. The brown triangles mark the molar ratios for the molecular formulas of higher masses assigned by MALDI-MS. Original 1,8-DHN solution: pH = 6.0, original 5,6-DHI solution: pH = 6.5, aged 1,8-DHN: pH = 7.0, aged 5,6-DHI: pH = 7.0.

3.2.2. MALDI-MS Results

Figure S7 shows the MALDI-MS mass spectra for oxidized and aged 5,6-DHI and 1,8-DHN samples with dark insoluble precipitates. For the MALDI-MS method, the dark-colored aged samples (~6 months old) were spotted onto the matrix (DHB). Figure S7 shows evidence of oxidation and potential oligomers (m/z: 296.2 for 5,6-DHI and m/z: 636.9 for 1,8-DHN) compared to the original masses of 149.1 Da for 5,6-DHI and 160.2 Da for 1,8-DHN. Aged 1,8-DHN samples showed ions with higher masses, 428.4 and 636.9, suggesting trimers and tetramers for 1,8-DHN. These results support the formation of oxidizing and aging 1,8-DHN or 5,6-DHI oligomers, like ESI-MS results.

3.3. Reduction Treatment Results

The responses of aged 1,8-DHN and 5,6-DHI samples to sodium dithionite and sodium borohydride treatments are shown in Figures S8 and S9. The reduced humic fractions of DOM are typically expected to show a significant loss of absorption (UVB and visible region) alongside significant fluorescence gain and a blue shift toward shorter wavelengths (Ma,

Del Vecchio et al., 2010). Figure S8 shows that all reduced 1,8-DHN and 5,6-DHI samples show an absorption loss in the UVB region and a decrease of absorption up to 500 nm for both borohydride-reduced 1,8-DHN and 5,6-DHI samples. However, dithionite-reduced 5,6-DHI only shows a noticeable absorption loss between 300–500 nm.

Figure S9 shows a fluorescence gain for all samples, up to ~2× fluorescence gain for aged 1,8-DHN reduced by sodium borohydride and up to ~4× fluorescence gain for aged 1,8-DHN reduced by sodium dithionite. Fluorescence gain due to reductions seems to be the least significant for aged 5,6-DHI reduced by borohydride, and about 30% for 5,6-DHI reduced by dithionite. Reduced 1,8-DHN samples show a blue shift of fluorescence (toward shorter wavelengths) in their normalized spectra compared to the pre-reduction samples.

4. Discussion

In this study, we demonstrate that humic optical properties can be reproduced by the oxidation of simple precursors. The crucial role of CDOM in the photochemistry of aquatic environments and nutrient balance in soils has led to increasing attempts to elucidate the molecular origins of DOMs absorbance and fluorescence properties. This study is an attempt to link the optical and molecular properties of DOM by transforming simple molecular structures through photo-oxidation and polymerization to develop humic properties. To mimic the optical properties of DOM, we selected two aromatic precursors that are analogous to common melanin precursors in natural environments to undergo oxidative polymerization [43]. The main objective is to evaluate how closely the substances generated by this process resemble DOMs optical properties. Optical measurements and mass spectrometry analysis were used to monitor and analyze the changes due to oxidation and polymerization of 1,8-DHN and 5,6-DHI. The interest in these aromatic precursors comes from the fact that 1,8-DHN and 5,6-DHI are both fungal melanin precursors [43]. Bell and Wheeler suggested that the complex dark-colored pigments from fungal melanin contribute to CDOM and its humic fractions of soils [16]. McKay found that once auto-oxidized, simple precursors such as hydroquinone can mimic humic-like optical properties detected in aquatic and terrestrial ecosystems [35]. The oxidized hydroquinone showed similar responses to treatments such as borohydride reduction, compared to DOM, which supports the role of charge-transfer interactions in the optical properties of DOM [35,54]. Leresche's computational approach to modeling the optical properties of DOM showed that using aromatic model chromophores and the superposition of their absorption spectra can reproduce DOMs featureless absorption trends [29].

Two views of the origins of humic optical properties include: (1) The optical properties of humic substances result from individual chromophore fractions adding up together [14,27]. In other words, the absorbance and fluorescence spectra of CDOM are formed because of the superposition of multiple individual chromophores [14,27,29]. (2) The newer view says that only a few chromophores are necessary to interact electronically (through charge-transfer interactions) and form the unique optical properties of CDOM [35,55,56]. Here, we investigate how simple chromophore precursors can evolve through oxidation and aging to mimic these optical properties. Our strategy supports both views, indicating: (1) The optical properties of humic substances can originate from multiple chromophoric compounds (oligomers with varying degrees of oxidation), and the sum of their absorbance and fluorescence results in humic-like optical properties. (2) The products of oxidative polymerization and aging process of fungal melanin model compounds (1–4 oligomeric units) could behave like charge transfer (CT) complexes in CDOM and produce humic absorbance and fluorescence trends. The applicability of the CT model was investigated by reduction treatments, showing similar responses associated with CT complexes in CDOM, which include loss of absorption, fluorescence gain, and a blue shift of fluorescence maxima.

For humic fractions of CDOM, the absorbance spectra show increasing values towards shorter wavelengths exponentially with no sharp peaks [56]. This characteristic is interpreted as the absorbance from the sum of the charge-transfer interactions of the chromophoric fractions to form the broad spectrum [27]. 1,8-DHN and 5,6-DHI showed

similar absorbance spectra after the oxidative polymerization and aging process (Figure 1). Continued oxidation and aging of 1,8-DHN precursors show an increase of absorption at 300–400 nm and the disappearance of 1,8-DHN's absorbance peaks at 302, 318, and 332 nm (Figure 1). A similar trend of absorbance changes occurred for 5,6-DHI samples over a shorter period (Figure 1). 5,6-DHI samples were aged for a shorter time compared to 1,8-DHN samples because dark-colored insoluble products were formed in 5,6-DHI samples in ~4 days. During the oxidative polymerization of 5,6-DHI, the oxidized oligomers are presumed to assemble and form large aggregates, developing dark-colored chromophores made of DHI species [57]. Both absorbance spectra show significant and continuous loss of distinct absorption peaks in the range of 28–340 nm and an increase in UVC absorptions (below 280 nm) after UV irradiation and during storage in the dark (Figures 1 and S2). The formation of oligomeric products of oxidative polymerization created new broad absorption trends decreasing with longer wavelengths, roughly exponentially. Figure 1 insets show the spectral slopes for aged 1,8-DHN and 5,6-DHI, which can be compared to Suwannee River HA (SRHA) as the standard sample (Figure S3). Aged 1,8-DHN samples with no H_2O_2 showed a log-linear decrease of absorption with a similar absorption slope (-0.011) to aged 5,6-DHI samples with no H_2O_2 (-0.010), whereas the spectral slope of SRHA is slightly steeper (-0.017) (Figure S3). The spectral slope of aged 5,6-DHI with 5% H_2O_2 was -0.013, close to SRHA. The spectral slopes between (-0.017)–(-0.010) are all within the same range as freshwater samples [58] and standard SRFA/SRHA samples [59], except for 1,8-DHN with 5% H_2O_2 that had the shallowest linear absorption trend with the slope of -0.0095.

For humic fractions of CDOM, absorption spectral slope has been used as a parameter to compare samples from different sources based on differences in molecular weight (MW) and natural processes such as photodegradation (photobleaching) [60,61]. Typically, the absorption slope shows negative correlations with the molecular weight of CDOM, which means higher molecular weights of CDOM show smaller values of absorption slopes [58,61]. The differences in spectral slopes for aged 1,8-DHN and 5,6-DHI with 5% H_2O_2 compared to SRHA confirms the negative correlation between spectral slope and molecular weight. MALDI-MS results in Figure S7 show the higher masses formed in aged 1,8-DHN with 5% H_2O_2 compared to aged 5,6-DHI with 5% H_2O_2. The spectral slope for aged 1,8-DHN with 5% H_2O_2 is shallower (-0.0095) compared to aged 5,6-DHI with 5% H_2O_2 (-0.0135) (Figure 1) and standard SRHA (-0.017), which is consistent with the formation of 1,8-DHN oligomers with higher molecular weights compared to aged 5,6-DHI samples. MALDI-MS results in Figure S7 show ions with higher masses (up to tetramers) in the range of 282.3–787.4 Da for aged 1,8-DHN with 5% H_2O_2, compared to 296.2–548.6 Da for aged 5,6-DHI with 5% H_2O_2. Overall, the spectral slopes were negatively correlated with molecular weight for aged 1,8-DHN and 5,6-DHI with 5% H_2O_2, consistent with higher masses in MALDI-MS results (Figure S7) and previously found correlations of CDOMs molecular weight and spectral slopes [58,61].

Reduction treatment of CDOM and its humic fractions is a useful approach to probe the molecular characteristics of the chromophoric fractions responsible for CDOMs absorbance and fluorescence properties [36,37,55]. Evidence of the presence of electron-donor and electron-acceptor moieties interacting electronically (CT model) has been confirmed by several studies on reduction treatments of CDOM [36,37,55]. Sodium borohydride is known to reduce aromatic aldehyde/ketone and quinones of CDOM and its humic isolates with irreversible loss of absorbance and gain in fluorescence intensities alongside a blue shift, while sodium dithionite is expected to selectively reduce quinones, causing loss of visible absorption and little changes to fluorescence, partially or completely reversible upon air exposure [35,36]. In the present work, to further evaluate the links between fungal melanin models and humic fractions of CDOM, the aged 1,8-DHN and 5,6-DHI samples were reduced by borohydride and dithionite, and absorbance and fluorescence spectra were collected. Like CDOM, a loss of absorbance because of reduction was observed in Figure S8. For 5,6-DHI reduced by dithionite, the loss of absorption was only evident

between 300–550 nm. Figure S9 highlights the fluorescence gain for reduced aged 1,8-DHN and 5,6-DHI samples, as well as a blue shift toward shorter wavelengths for both reduced 1,8-DHN samples. Del Vecchio and Schendorf found that dithionite reduction did not result in any significant changes of fluorescence for the standard lignin model compounds and SRFA; however, Elliot soil humic acid (ESHA) standard responded to reduction treatments by showing fluorescence gain and a blue shift [36]. Figure S9 shows that borohydride and dithionite-reduced 1,8-DHN showed a significant fluorescence gain and a blue shift, like the responses of reduced ESHA. Borohydride and dithionite-reduced 5,6-DHI samples showed fluorescence gains with no noticeable blue shift. Considering the aromatic nature of our precursors and the oxidative polymerization approach, the similar responses of our aged fungal melanin models support the significant contribution of aromatic moieties of CDOM to its optical characteristics, especially to its fluorescence, by resulting in fluorescence gain and a blue shift of the emission trends [37]. These findings are consistent with the CT model explaining the origins of the optical properties of CDOM and its standard isolates, providing further evidence that fungal melanin models could mimic humic optical properties, fitting into both superposition and CT models. The resemblance of the responses to reduction between ESHA [36] and aged 1,8-DHN could also be interpreted as evidence indicating the contribution of fungal melanin with 1,8-DHN building units to ESHA and its humic optical trends.

Specific UV absorbance (SUVA) at 254 nm is a common metric used to characterize humic fractions of CDOM. SUVA is calculated by dividing the absorbance values by the estimated concentration of dissolved organic carbon (DOC) in the samples [62]. SUVA measurements at 254 nm are often correlated with the degree of aromaticity for marine CDOM samples [62]. SUVA values at 254 nm show the absorbance of DOM per unit of carbon, assuming aromatic fractions of DOM contribute strongly to this signal. Therefore, SUVA values at 254 can be used as "surrogate" measurements for the contents of aromatic carbon in both terrestrial and marine DOC fractions of DOM [63]. As DOM becomes more processed, moving through the atmosphere and marine environments, SUVA values increase [64]. Typically, high SUVA values are interpreted as high inputs from terrestrial environments and increased microbial degradation [64]. The SUVA value for the 1,8-DHN sample at 254 nm was estimated as 7.75 L/mg·m (Figure S4). This SUVA value is higher than freshwater and seawater samples [58]. Marine DOM shows SUVA in the range of 0–4.5, whereas SUVA values for terrestrial DOM can average up to 6.0 [64]. SUVA value of 7.75 L/mg·m for aged 1,8-DHN, higher than average SUVA of marine and terrestrial DOM [64], is consistent with a higher degree of aromaticity in aged 1,8-DHN. This observation is expected because natural humic substances also have aliphatic portions, which are non-absorbing in optical measurements [65].

For humic fractions of CDOM, the fluorescence measurements show broad peaks within the range of 400–500 nm, which shift towards longer wavelengths with varying excitation wavelengths (300–600 nm) [56]. The emission spectra of 1,8-DHN and 5,6-DHI samples were collected for untreated, oxidized, and aged samples throughout the storage period. Figure 2 shows that for all 1,8-DHN samples, the fluorescence intensity decreases after UV irradiation, and it continues to decrease during 10 days of storage in the dark. The fluorescence intensities decreased by ~4× for aged 1,8-DHN and 5,6-DHI and ~9× for aged 1,8-DHN and 5,6-DHI with 5% H_2O_2, for 1,8-DHN samples with 5% H_2O_2, new broad peaks that were shifted toward longer wavelengths were detected (Figure 2). Figure 2 shows that the emission spectrum for 5,6-DHI samples also shifted towards longer wavelengths (redshift) like 1.8-DHN samples. Overall, the emission spectral trends for aged 1,8-DHN and 5,6-DHI samples resemble the humic emission spectra (Figure S5). To compare the emission peaks within a broad range of excitation wavelengths, emission spectra were plotted for the same aged 1,8-DHN and 5,6-DHI samples. Figure S5 shows redshifts towards longer excitation wavelengths for both samples; however, 5,6-DHI also shows lower-intensity emission peaks that are different from humic samples. Overall, the emission spectra for aged 1,8-DHN samples were more like Suwannee River HA, which

is consistent with the "superposition model", where the sum of multiple chromophoric structures such as oligomers with varying degrees of oxidation show broad humic-like absorbance and fluorescence trends.

Negative-mode ESI results for 1,8-DHN samples with H_2O_2 show evidence of ions with higher masses compared to the original precursor for all samples in both KMD plots and the mass spectra (Figure 3 and Figure S6). Specifically, tetramers were formed as new clusters in the mass spectra and KMD plots for aged 1,8-DHN with 5% H_2O_2 (Figures 3 and S6). As it was expected, KMD plots for our oxidized and aged samples helped visualize the evidence for oligomerization by showing four distinct repeat units for aged 1,8-DHN with 5% H_2O_2 (Figure S6). These results for aged 1,8-DHN samples can be coupled with its optical characterization to support our initial hypothesis that oxidative polymerization of a simple fungal melanin precursor forming only up to four units can mimic humic properties. One mechanism for the formation of humic substances is the formation of phenolic radicals and their oxidative polymerization in soil [66,67]. The oxidative polymerization products could be produced by enzymatic reactions (e.g., peroxidase) [68] and degradations by the fungi in soil (e.g., white rot) [69,70]. Our focus in this study was to use mass spectrometry analysis to find evidence of oxidized and aged oligomers of 1,8-DHN and 5,6-DHI precursors mimicking humic optical properties. Therefore, our mass spectrometry results were naturally less complex, with lower mass ranges and fewer m/z peaks in Figure 3, compared to aquatic or terrestrial CDOM and its humic fractions [39]. All negative-mode ESI mass spectra for aged 1,8-DHN show the base peak m/z: 159.04, which shows the detection of negatively charged ions of 1,8-DHN molecules with an original molar mass of 160.17 g/mole. Other than the 1,8-DHN formula being the most common (C10H8O2) with m/z: 159.04 for negative-mode ESI, the second most abundant peaks have m/z: 325.18 with $C_{20}H_{22}O_4$, a dimer of 1,8-DHN. Ions with m/z: 317.08, 333.07, and 347.05 with assigned formulas of $C_{20}H_{14}O_4$ and $C_{20}H_{14}O_5$, and $C_{20}H_{12}O_6$ show more evidence of potential dimers of 1,8-DHN and its oxidized forms. One of the highest masses formed is m/z: 523.10 with a molecular formula of $C_{30}H_{20}O_9$, as a possible oxidized trimer of 1,8-DHN. Figure 3 shows the formation of clusters with higher masses for aged 5,6-DHI, compared to the original 5,6-DHI with m/z of 149.04 and the original formula of $C_8H_7NO_2$. The most abundant molecular formula of aged 5,6-DHI is $C_{16}H_{14}N_2O_4$ with m/z: 297.08, as a potential dimer of 5,6-DHI. Ion with m/z: 200.07 ($C_8H_{13}NO_2$ with m/z: 155 Da) shows hydrogenation of 5,6-DHI and addition of CO_2 (m/z: 155 Da + m/z of CO_2: 44 Da), consistent with some of the higher H/C and O/C values in Figure 4. Ions with m/z: 293.05 ($C_{16}H_{10}N_2O_4$) and 329.04 ($C_{16}H_{14}N_2O_6$) show evidence of oxidized dimers of 5,6-DHI. One of the highest masses formed, m/z: 414.21 ($C_{24}H_{21}N_3O_4$), could be part of a 5,6-DHI trimer ion. Tables S1 and S2 summarize the most abundant molecular formulas assigned to aged 1,8-DHN and 5,6-DHI.

Considering the chemical variability and complexity of the mass spectrometry data for DOM and its standard references, a useful approach is to compare ranges of molar ratios representing their most common molecular formulas. Kim studied the molecular characteristics of SRFA and SRHA [41] and found the following ranges of molar ratios: O/C: 0.20–0.75 and H/C: 0.5–1.5. SRFA and SRHA are commonly analyzed isolates of DOM, differentiated by their solubility at different pH levels. Figure 4 shows that these ranges encompass most of the common molecular formulas (purple circles) in the van Krevelen diagram for aged 1,8-DHN and 5,6-DHI. The number of molecular formulas assigned to aged 5,6-DHI and 1,8-DHN were 1187 and 400. The purple SRHA/SRFA region encompasses over 90% of those formulas, with some formulas having higher O/C for both 1,8-DHN and 5,6-DHI and some having lower H/C and O/C for aged 5,6-DHI, falling outside of the SRFA/SRHA regions. These differences could be linked to the presence of H_2O_2 in the samples, resulting in higher O/C values and higher aromaticity of aged 5,6-DHI, showing lower H/C and O/C compared to the SRFA/SRHA region. All samples show a shift towards higher O/C (following the black arrow), which is consistent with the expected oxidation; however, this shift toward higher O/C appears more frequently in the right-side plots,

consistent with the addition of H_2O_2. For 5,6-DHI samples, some hydrogenation (higher H/C, orange upward arrow) is suggested, alongside the diagonal grey arrow suggesting hydration. The blue arrow could be indicating the oxidative polymerization of original precursors following the diagonal line, while H/C decreases (loss of hydrogen due to the presence of hydroxyl radicals) and O/C increases (oxidation). Mass spectrometry studies of oxidative polymerization and formation of 1,8-DHN oligomers show that in negative-mode ESI, loss of hydrogen is expected after ionization, alongside the expected C-C and C-O bond formations by oligomers [43]. These reaction pathways are merely qualitative to investigate possible transformations of natural organic matter [51]. The red marked areas show the molar ratios for synthetic melanin and humic-like substances with 5,6-DHI and 1,8-DHN building blocks, with O/C = 0.25 and H/C = 0.78–0.79 [49,50], encompassing many of assigned molecular formulas in Figure 4. The black diamond shapes mark the molar ratios for the original precursors, confirming the presence of original 1,8-DHN and 5,6-DHI molecules in several points in Figure 4. The black star represents the molar ratios of dimers, showing that the formation of dimers is confirmed by molecular formula assignments, and the orange hexagons show the ranges of molar ratios for the most abundant molecular formulas summarized in Tables S1 and S2. The brown triangles mark the molar ratios for higher masses in MALDI-MS results, highlighted for comparison, noting that MALDI-MS samples were aged for ~6 months, containing precipitates with higher masses. Therefore, some of the MALDI-MS molar ratios do not overlap with assigned ESI-MS formulas to the samples aged for ~10 days (Figure 4).

MALDI-MS was selected to couple with ESI-MS results to improve the detection of larger oxidized oligomers in the aged samples. MALDI-MS results also showed evidence of oligomers formed with higher masses (Figure S7). For aged 5,6-DHI, m/z: 296.2 is likely to be representing the formula of $C_{16}H_{12}N_2O_4$, and m/z 302.3 and 366.4 could be assigned to $C_{16}H_{18}N_2O_4$ and $C_{16}H_6N_4O_7$, which show evidence of oxidation and dimers of 5,6-DHI. The highest mass for 5,6-DHI in the MALDI-MS mass spectrum is m/z:548.6, potentially showing a tetramer of 5,6-DHI ($C_32H_{12}N_4O_8$). One of the major m/z peaks of the 1,8-DHN's MALDI mass spectrum is 549.1, which could be assigned to $C_{30}H_{24}O_6$ as the trimer of 1,8-DHN. Ions with m/z: 282.3, 366.5, 636.5 are likely to be $C_{19}H_{10}O_2$ (dimer with loss of CO_2/H_2O), $C_{20}H_{28}O_6$ and $C_{40}H_{38}O_8$ as potential trimers and tetramers of 1,8-DHN. Based on the general definition of fungal melanin consisting of 4–8 monomer units [71], MALDI mass spectrometry of our aged 1,8-DHN and 5,6-DHI samples shows evidence of oxidized melanin oligomers up to 4 units (tetramers with m/z: 636.9). Typical examples of the assigned molecular formulas to standard HA by high-resolution mass spectrometry include $C_{16}H_{13}O_{12}$, $C_{18}H_{21}O_{10}$, and $C_{20}H_{22}NO_8$ [72,73], comparable to the suggested molecular formulas for our aged samples. Overall, the mass spectrometry results showed evidence of oxidative polymerization of 1,8-DHN and 5,6-DHI, where up to 4 oligomeric units (tetramers) were formed for 1,8-DHN with 5% H_2O_2. For 5,6-DHI samples, the results showed some ions with higher masses (dimers) and varying degrees of oxidation, but the results were not as straightforward because of the insolubility of 5,6-DHI's oxidative polymerization products. The growth of small 5,6-DHI oligomers (e.g., dimers, trimers, etc.) starts slowly, but then these small oligomers grow into larger aggregates, which assemble (i.e., self-assembly) and form dark insoluble precipitates over several days [57,74].

5. Conclusions

Our findings show that oxidative polymerization of 1,8-DHN and 5,6-DHI as fungal melanin precursors reproduces optical characteristics of humic fractions of CDOM. In this study, 1,8-DHN samples were successfully oxidized and polymerized after UV irradiation and aging. 5,6-DHI samples initially showed a similar trend to 1,8-DHN, but the aging process resulted in the formation of dark insoluble precipitates. Absorbance spectra of 1,8-DHN and 5,6-DHI showed significant loss of absorbance, the disappearance of original absorbance peaks, and an overall shift towards a broad and featureless humic-like absorbance spectrum. Fluorescence spectra likewise showed shifts towards longer wave-

lengths (redshifts), turning into broad peaks from 400–500 nm, which is another attribute of the humic substances. Humic-like optical properties of CDOM reproduced by the aged 1,8-DHN and 5,6-DHI can be explained by the superposition model, the sum of oligomers with varying degrees of oxidation forming humic optical trends, and the CT model, possible CT interactions revealed by reduction treatments resulting in broad absorption and fluorescence trends. Mass spectrometry results showed evidence of 1,8-DHN dimers, trimers, and tetramers being formed. Adding H_2O_2 as an oxidizing agent resulted in accelerated oxidative polymerization, as observed in negative-mode ESI mass spectra. However, mass spectrometry results of aged 5,6-DHI samples were more complex due to the formation of dark-colored insoluble precipitates during the experiments. Overall, absorbance and fluorescence spectra of oxidized 1,8-DHN and 5,6-DHI over time showed similarities in their trends compared to the absorbance and fluorescence spectra of humic fractions of CDOM. In conclusion, the results of optical and molecular characterization of oxidative polymerization of 1,8-DHN and 5,6-DHI show that only about 1–4 units of oligomers with varying degrees of oxidation mimicked the optical properties of humic fractions of CDOM. This supports our hypothesis that we could mimic humic properties by oxidizing and aging simple melanin precursors.

Supplementary Materials: The following supporting information can be downloaded at: https://www.mdpi.com/article/10.3390/w15071400/s1, Figure S1: Absorption changes (Δ(Abs)) for aged 1,8-DHN and 5,6-DHI at 350 nm and 400 nm over time; Figure S2: Absorbance spectra of 1,8-DHN and 5,6-DHI, no H_2O_2, and with 5% H_2O_2; Figure S3: Absorbance spectrum and log-linear absorption plot of Suwannee River humic acid (SRHA); Figure S4: Specific absorbance of the aged 1,8-DHN sample (~6 months) per estimated DOC (mg/L); Figure S5: Flattened excitation-emission matrix (EEM) plots for aged 1,8-DHN, aged 5,6-DHI, and SRHA; Figure S6: KMD plots for post-irradiation samples of 1,8-DHN and 5,6-DHI, with or without 5% H_2O_2; Figure S7: Mass spectra of oxidized and aged 5,6-DHI and 1,8-DHN (MALDI); Table S1: Molecular formulas assigned to ESI-MS results for aged 5,6-DHI + 5% H_2O_2; Table S2: Molecular formulas assigned to ESI-MS results for aged 1,8-DHN + 5% H_2O_2; Figure S8: Absorbance spectra of aged 1,8-DHN and 5,6-DHI, treated with sodium borohydride and sodium dithionite; Figure S9: Fluorescence spectra of aged 1,8-DHN and 5,6-DHI, treated with sodium borohydride and sodium dithionite.

Author Contributions: Conceptualization, N.K. and S.A.G.; methodology, N.K. and S.A.G.; software, N.K.; validation, N.K. and S.A.G.; formal analysis, N.K.; investigation, N.K. and S.A.G.; resources, S.A.G.; data curation, N.K.; writing—original draft preparation, N.K.; writing—review and editing, N.K. and S.A.G.; visualization, N.K.; supervision, S.A.G.; project administration, S.A.G.; funding acquisition, S.A.G. All authors have read and agreed to the published version of the manuscript.

Data Availability Statement: The data presented in this study are available on request from the corresponding authors. The data are not publicly available due to privacy.

Conflicts of Interest: The authors declare no conflict of interest.

References

1. Senesi, N.; Loffredo, E. The chemistry of soil organic matter. In *Soil Physical Chemistry*; CRC Press: Boca Raton, FL, USA, 2018; pp. 239–370. ISBN 9780203739280.
2. Schnitzer, M. Soil organic matter—The next 75 years. *Soil Sci.* **1991**, *151*, 41–58. [CrossRef]
3. Högberg, M.N.; Skyllberg, U.; Högberg, P.; Knicker, H. Does ectomycorrhiza have a universal key role the formation of soil organic matter in boreal forests? *Soil Biol. Biochem.* **2020**, *140*, 107635. [CrossRef]
4. Poage, M.A.; Feng, X. A theoretical analysis of steady state δ13C profiles of soil organic matter. *Glob. Biogeochem. Cycles* **2004**, *18*. [CrossRef]

5. Friedlingstein, P.; O'sullivan, M.; Jones, M.W.; Andrew, R.M.; Gregor, L.; Hauck, J.; Le Quéré, C.; Luijkx, I.T.; Olsen, A.; Peters, G.P. Global carbon budget 2022. *Earth Syst. Sci. Data.* **2022**, *14*, 4811–4900. [CrossRef]
6. Fellman, J.B.; D'Amore, D.V.; Hood, E.; Boone, R.D. Fluorescence characteristics and biodegradability of dissolved organic matter in forest and wetland soils from coastal temperate watersheds in southeast Alaska. *Biogeochemistry* **2008**, *88*, 169–184. [CrossRef]
7. Hansell, D.A.; Carlson, C.A. *Biogeochemistry of Marine Dissolved Organic Matter*; Academic Press: Cambridge, MA, USA, 2014; ISBN 978-0-12-405940-5.
8. Welikala, D.; Hucker, C.; Hartland, A.; Robinson, B.H.; Lehto, N.J. Trace metal mobilization by organic soil amendments: Insights gained from analyses of solid and solution phase complexation of cadmium, nickel and zinc. *Chemosphere* **2018**, *199*, 684–693. [CrossRef]
9. Jaffé, R.; McKnight, D.; Maie, N.; Cory, R.; McDowell, W.; Campbell, J. Spatial and temporal variations in DOM composition in ecosystems: The importance of long-term monitoring of optical properties. *J. Geophys. Res. Biogeosci.* **2008**, *113*. [CrossRef]
10. Siletti, C.E.; Zeiner, C.A.; Bhatnagar, J.M. Distributions of fungal melanin across species and soils. *Soil Biol. Biochem.* **2017**, *113*, 285–293. [CrossRef]
11. Kögel-Knabner, I. The macromolecular organic composition of plant and microbial residues as inputs to soil organic matter. *Soil Biol. Biochem.* **2002**, *34*, 139–162. [CrossRef]
12. Leenheer, J.A.; Croué, J.-P. Peer reviewed: Characterizing aquatic dissolved organic matter. *Environ. Sci. Technol.* **2003**, *37*, 18A–26A. [CrossRef]
13. Astoreca, R.; Rousseau, V.; Lancelot, C. Coloured dissolved organic matter (CDOM) in Southern North Sea waters: Optical characterization and possible origin. *Estuar. Coast. Shelf Sci.* **2009**, *85*, 633–640. [CrossRef]
14. Stedmon, C.A.; Markager, S.; Bro, R. Tracing dissolved organic matter in aquatic environments using a new approach to fluorescence spectroscopy. *Mar. Chem.* **2003**, *82*, 239–254. [CrossRef]
15. Zhang, Y.; Zhou, L.; Zhou, Y.; Zhang, L.; Yao, X.; Shi, K.; Jeppesen, E.; Yu, Q.; Zhu, W. Chromophoric dissolved organic matter in inland waters: Present knowledge and future challenges. *Sci. Total Environ.* **2021**, *759*, 143550. [CrossRef] [PubMed]
16. Bell, A.A.; Wheeler, M.H. Biosynthesis and functions of fungal melanins. *Annu. Rev. Phytopathol.* **1986**, *24*, 411–451. [CrossRef]
17. Skinner, C. The Occurrence in Soil of Bacteria, Actinomycetes, and Molds Capable of Transforming Tyrosine to Melanin or Other Pigments1. *Soil Sci. Soc. Am. J.* **1940**, *4*, 231. [CrossRef]
18. Butler, M.; Day, A. Fungal melanins: A review. *Can. J. Microbiol.* **1998**, *44*, 1115–1136. [CrossRef]
19. Frey, S.D. Mycorrhizal fungi as mediators of soil organic matter dynamics. *Annu. Rev. Ecol. Evol. Syst.* **2019**, *50*, 237–259. [CrossRef]
20. Cao, W.; Zhou, X.; McCallum, N.C.; Hu, Z.; Ni, Q.Z.; Kapoor, U.; Heil, C.M.; Cay, K.S.; Zand, T.; Mantanona, A.J. Unraveling the structure and function of melanin through synthesis. *J. Am. Chem. Soc.* **2021**, *143*, 2622–2637. [CrossRef]
21. Sun, S.; Zhang, X.; Sun, S.; Zhang, L.; Shan, S.; Zhu, H. Production of natural melanin by Auricularia auricula and study on its molecular structure. *Food Chem.* **2016**, *190*, 801–807. [CrossRef]
22. Bianca, M.R.; Baluha, D.R.; Gonsior, M.; Schmitt-Kopplin, P.; Del Vecchio, R.; Blough, N.V. Contribution of ketone/aldehyde-containing compounds to the composition and optical properties of Suwannee River fulvic acid revealed by ultrahigh resolution mass spectrometry and deuterium labeling. *Anal. Bioanal. Chem.* **2020**, *412*, 1441–1451. [CrossRef]
23. d'Ischia, M.; Napolitano, A.; Ball, V.; Chen, C.-T.; Buehler, M.J. Polydopamine and eumelanin: From structure–property relationships to a unified tailoring strategy. *Acc. Chem. Res.* **2014**, *47*, 3541–3550. [CrossRef] [PubMed]
24. Dalzell, B.; Minor, E.; Mopper, K. Photodegradation of estuarine dissolved organic matter: A multi-method assessment of DOM transformation. *Org. Geochem.* **2009**, *40*, 243–257. [CrossRef]
25. Dittmar, T.; Lennartz, S.T.; Buck-Wiese, H.; Hansell, D.A.; Santinelli, C.; Vanni, C.; Blasius, B.; Hehemann, J.-H. Enigmatic Persistence of Dissolved Organic Matter in the Ocean. *Nat. Rev. Earth Environ.* **2021**, *2*, 570–583. Available online: https://www.nature.com/natreveearthenviron (accessed on 1 February 2023). [CrossRef]
26. Sharpless, C.M.; Blough, N.V. The importance of charge-transfer interactions in determining chromophoric dissolved organic matter (CDOM) optical and photochemical properties. *Environ. Sci. Process. Impacts* **2014**, *16*, 654–671. [CrossRef]
27. Del Vecchio, R.; Blough, N.V. On the origin of the optical properties of humic substances. *Environ. Sci. Technol.* **2004**, *38*, 3885–3891. [CrossRef] [PubMed]
28. Zonios, G.; Dimou, A. Melanin optical properties provide evidence for chemical and structural disorder in vivo. *Opt. Express* **2008**, *16*, 8263–8268. [CrossRef]
29. Leresche, F.; Vialykh, E.A.; Rosario-Ortiz, F.L. Computational Calculation of Dissolved Organic Matter Absorption Spectra. *Environ. Sci. Technol.* **2021**, *56*, 491–500. [CrossRef] [PubMed]
30. Wang, J.; Blancafort, L. Stability and optical absorption of a comprehensive virtual library of minimal eumelanin oligomer models. *Angew. Chem. Int. Ed.* **2021**, *60*, 18800–18809. [CrossRef]
31. Perna, G.; Palazzo, G.; Mallardi, A.; Capozzi, V. Fluorescence properties of natural eumelanin biopolymer. *J. Lumin.* **2011**, *131*, 1584–1588. [CrossRef]
32. Nighswander-Rempel, S.P.; Riesz, J.; Gilmore, J.; Meredith, P. A quantum yield map for synthetic eumelanin. *J. Chem. Phys.* **2005**, *123*, 194901. [CrossRef]
33. Meredith, P.; Riesz, J. Radiative Relaxation Quantum Yields for Synthetic Eumelanin. *Photochem. Photobiol.* **2004**, *79*, 211–216. [CrossRef] [PubMed]

34. Meredith, P.; Sarna, T. The physical and chemical properties of eumelanin. *Pigment Cell Res.* **2006**, *19*, 572–594. [CrossRef] [PubMed]

35. McKay, G. Autoxidized hydroquinone mimics the optical properties of chromophoric dissolved organic matter. *Environ. Sci. Technol. Lett.* **2021**, *8*, 825–831. [CrossRef]

36. Li, H.; McKay, G. Relationships between the physicochemical properties of dissolved organic matter and its reaction with sodium borohydride. *Environ. Sci. Technol.* **2021**, *55*, 10843–10851. [CrossRef]

37. Del Vecchio, R.; Schendorf, T.M.; Blough, N.V. Contribution of quinones and ketones/aldehydes to the optical properties of humic substances (HS) and chromophoric dissolved organic matter (CDOM). *Environ. Sci. Technol.* **2017**, *51*, 13624–13632. [CrossRef]

38. Yakimov, B.P. Oxidation of individual aromatic species gives rise to humic-like optical properties. *Environ. Sci. Technol. Lett.* **2022**, *9*, 452–458. [CrossRef]

39. Hertkorn, N.; Frommberger, M.; Witt, M.; Koch, B.P.; Schmitt-Kopplin, P.; Perdue, E.M. Natural organic matter and the event horizon of mass spectrometry. *Anal. Chem.* **2008**, *80*, 8908–8919. [CrossRef]

40. Hawkes, J.A.; d'Andrilli, J.; Agar, J.N.; Barrow, M.P.; Berg, S.M.; Catalán, N.; Chen, H.; Chu, R.K.; Cole, R.B.; Dittmar, T. An international laboratory comparison of dissolved organic matter composition by high resolution mass spectrometry: Are we getting the same answer? Limnol. *Oceanogr. Meth.* **2020**, *18*, 235–258. [CrossRef]

41. Kim, S.; Kim, D.; Jung, M.J.; Kim, S. Analysis of environmental organic matters by Ultrahigh-Resolution mass spectrometry—A review on the development of analytical methods. *Mass Spectrom. Rev.* **2022**, *41*, 352–369. [CrossRef] [PubMed]

42. Baluha, D.R.; Blough, N.V.; Del Vecchio, R. Selective mass labeling for linking the optical properties of chromophoric dissolved organic matter to structure and composition via ultrahigh resolution electrospray ionization mass spectrometry. *Environ. Sci. Technol.* **2013**, *47*, 9891–9897. [CrossRef]

43. Cecchini, M.M.; Reale, S.; Manini, P.; d'Ischia, M.; De Angelis, F. Modeling Fungal Melanin Buildup: Biomimetic Polymerization of 1,8-Dihydroxynaphthalene Mapped by Mass Spectrometry. *Chem. Eur. J.* **2017**, *23*, 8092–8098. [CrossRef] [PubMed]

44. Navalon, S.; Alvaro, M.; Alcaina, I.; Garcia, H. Multi-method characterization of DOM from the Turia river (Spain). *Appl. Geochem.* **2010**, *25*, 1632–1643. [CrossRef]

45. Banerjee, A.; Supakar, S.; Banerjee, R. Melanin from the nitrogen-fixing bacterium Azotobacter chroococcum: A spectroscopic characterization. *PLoS ONE* **2014**, *9*, e84574. [CrossRef] [PubMed]

46. Pralea, I.-E.; Moldovan, R.-C.; Petrache, A.-M.; Ilieș, M.; Hegheș, S.-C.; Ielciu, I.; Nicoară, R.; Moldovan, M.; Ene, M.; Radu, M. From extraction to advanced analytical methods: The challenges of melanin analysis. *Int. J. Mol. Sci.* **2019**, *20*, 3943. [CrossRef]

47. Ye, M.; Guo, G.-Y.; Lu, Y.; Song, S.; Wang, H.-Y.; Yang, L. Purification, structure and anti-radiation activity of melanin from Lachnum YM404. *Int. J. Biol. Macromol.* **2014**, *63*, 170–176. [CrossRef]

48. Babitskaya, V.; Shcherba, V.; Lkonnikova, N. Melanin complex of the fungusInonotus obliquus. *Appl. Biochem. Microbiol.* **2000**, *36*, 377–381. [CrossRef]

49. Yoon, H.Y.; Jeong, H.J.; Cha, J.-Y.; Choi, M.; Jang, K.-S.; Kim, W.-Y.; Kim, M.G.; Jeon, J.-R. Structural variation of humic-like substances and its impact on plant stimulation: Implication for structure-function relationship of soil organic matters. *Sci. Total Environ.* **2020**, *725*, 138409. [CrossRef]

50. Park, H.; Yang, I.; Choi, M.; Jang, K.-S.; Jung, J.C.; Choi, K.-Y. Engineering of melanin biopolymer by co-expression of MelC tyrosinase with CYP102G4 monooxygenase: Structural composition understanding by 15 tesla FT-ICR MS analysis. *Biochem. Eng. J.* **2020**, *157*, 107530. [CrossRef]

51. Kim, S.; Simpson, A.J.; Kujawinski, E.B.; Freitas, M.A.; Hatcher, P.G. High resolution electrospray ionization mass spectrometry and 2D solution NMR for the analysis of DOM extracted by C18 solid phase disk. *Org. Geochem.* **2003**, *34*, 1325–1335. [CrossRef]

52. Schendorf, T.M.; Del Vecchio, R.; Koech, K.; Blough, N.V. A standard protocol for NaBH4 reduction of CDOM and HS. *Limnol. Oceanogr. Meth.* **2016**, *14*, 414–423. [CrossRef]

53. Schum, S.K.; Brown, L.E.; Mazzoleni, L.R. MFAssignR: Molecular formula assignment software for ultrahigh resolution mass spectrometry analysis of environmental complex mixtures. *Environ. Res.* **2020**, *191*, 110114. [CrossRef] [PubMed]

54. Cory, R.M.; McKnight, D.M. Fluorescence spectroscopy reveals ubiquitous presence of oxidized and reduced quinones in dissolved organic matter. *Environ. Sci. Technol.* **2005**, *39*, 8142–8149. [CrossRef] [PubMed]

55. Ma, J.; Del Vecchio, R.; Golanoski, K.S.; Boyle, E.S.; Blough, N.V. Optical properties of humic substances and CDOM: Effects of borohydride reduction. *Environ. Sci. Technol.* **2010**, *44*, 5395–5402. [CrossRef]

56. Andrew, A.A.; Del Vecchio, R.; Subramaniam, A.; Blough, N.V. Chromophoric dissolved organic matter (CDOM) in the Equatorial Atlantic Ocean: Optical properties and their relation to CDOM structure and source. *Mar. Chem.* **2013**, *148*, 33–43. [CrossRef]

57. Arzillo, M.; Mangiapia, G.; Pezzella, A.; Heenan, R.K.; Radulescu, A.; Paduano, L.; d'Ischia, M. Eumelanin buildup on the nanoscale: Aggregate growth/assembly and visible absorption development in biomimetic 5, 6-dihydroxyindole polymerization. *Biomacromolecules* **2012**, *13*, 2379–2390. [CrossRef]

58. Chen, H.; Zheng, B.; Song, Y.; Qin, Y. Correlation between molecular absorption spectral slope ratios and fluorescence humification indices in characterizing CDOM. *Aquat. Sci.* **2011**, *73*, 103–112. [CrossRef]

59. Rodríguez, F.J.; Schlenger, P.; García-Valverde, M. Monitoring changes in the structure and properties of humic substances following ozonation using UV–Vis, FTIR and 1H NMR techniques. *Sci. Total Environ.* **2016**, *541*, 623–637. [CrossRef]

60. Yacobi, Y.Z.; Alberts, J.J.; Takacs, M.; McElvaine, M.L. Absorption spectroscopy of colored dissolved organic carbon in Georgia (USA) rivers: The impact of molecular size distribution. *J. Limnol.* **2003**, *62*, 41–46. [CrossRef]

61. Helms, J.R.; Stubbins, A.; Ritchie, J.D.; Minor, E.C.; Kieber, D.J.; Mopper, K. Absorption spectral slopes and slope ratios as indicators of molecular weight, source, and photobleaching of chromophoric dissolved organic matter. *Limnol. Oceanogr.* **2008**, *53*, 955–969. [CrossRef]

62. Weishaar, J.L.; Aiken, G.R.; Bergamaschi, B.A.; Fram, M.S.; Fujii, R.; Mopper, K. Evaluation of specific ultraviolet absorbance as an indicator of the chemical composition and reactivity of dissolved organic carbon. *Environ. Sci. Technol.* **2003**, *37*, 4702–4708. [CrossRef]

63. Traina, S.J.; Novak, J.; Smeck, N.E. An ultraviolet absorbance method of estimating the percent aromatic carbon content of humic acids. *J. Environ. Qual.* **1990**, *19*, 151–153. [CrossRef]

64. D'Andrilli, J.; Silverman, V.; Buckley, S.; Rosario-Ortiz, F.L. Inferring ecosystem function from dissolved organic matter optical properties: A critical review. *Environ. Sci. Technol.* **2022**, *56*, 11146–11161. [CrossRef] [PubMed]

65. McDonald, S.; Bishop, A.G.; Prenzler, P.D.; Robards, K. Analytical chemistry of freshwater humic substances. *Anal. Chim. Acta* **2004**, *527*, 105–124. [CrossRef]

66. Cozzolino, A.; Piccolo, A. Polymerization of dissolved humic substances catalyzed by peroxidase. Effects of pH and humic composition. *Org. Geochem.* **2002**, *33*, 281–294. [CrossRef]

67. Olk, D.; Bloom, P.; Perdue, E.; McKnight, D.; Chen, Y.; Farenhorst, A.; Senesi, N.; Chin, Y.P.; Schmitt-Kopplin, P.; Hertkorn, N. Environmental and agricultural relevance of humic fractions extracted by alkali from soils and natural waters. *J. Environ. Qual.* **2019**, *48*, 217–232. [CrossRef]

68. Piccolo, A.; Cozzolino, A.; Conte, P.; Spaccini, R. Polymerization of humic substances by an enzyme-catalyzed oxidative coupling. *Naturwissenschaften* **2000**, *87*, 391–394. [CrossRef]

69. Haider, K.M.; Martin, J.P. Mineralization of 14C-labelled humic acids and of humic-acid bound 14C-xenobiotics by Phanerochaete chrysosporium. Soil Biol. *Biochem.* **1988**, *20*, 425–429. [CrossRef]

70. Steffen, K.T.; Hatakka, A.; Hofrichter, M. Degradation of humic acids by the litter-decomposing basidiomycete Collybia dryophila. *Appl. Environ. Microbiol.* **2002**, *68*, 3442–3448. [CrossRef]

71. Watt, A.A.; Bothma, J.P.; Meredith, P. The supramolecular structure of melanin. *Soft Matter* **2009**, *5*, 3754–3760. [CrossRef]

72. Stenson, A.C.; Marshall, A.G.; Cooper, W.T. Exact masses and chemical formulas of individual Suwannee River fulvic acids from ultrahigh resolution electrospray ionization Fourier transform ion cyclotron resonance mass spectra. *Anal. Chem.* **2003**, *75*, 1275–1284. [CrossRef]

73. Zhang, X.; Kang, J.; Chu, W.; Zhao, S.; Shen, J.; Chen, Z. Spectral and mass spectrometric characteristics of different molecular weight fractions of dissolved organic matter. *Sep. Purif. Technol.* **2020**, *253*, 117390. [CrossRef]

74. Bridelli, M.G. Self-assembly of melanin studied by laser light scattering. *Biophys. Chem.* **1998**, *73*, 227–239. [CrossRef] [PubMed]